Open access • Journal Article • DOI:10.1103/PHYSREVB.64.235305

Band structure of MoS 2 , MoSe 2 , and α – MoTe 2 : Angle-resolved photoelectron spectroscopy and ab initio calculations — Source link

Th. Böker, R. Severin, A. Müller, Christoph Janowitz ...+5 more authors

Institutions: Humboldt University of Berlin, University of Münster

Published on: 15 Nov 2001 - Physical Review B (American Physical Society)

Band structure of MoS_2, $MoSe_2$, and α-$MoTe_2$: Angle-resolved photoelectron spectroscopy and *ab initio* calculations

Th. Böker, R. Severin, A. Müller, C. Janowitz, and R. Manzke
Institut für Physik, Humboldt-Universität zu Berlin, Invalidenstraße 110, 10115 Berlin

D. Voß, P. Krüger, A. Mazur, and J. Pollmann
Institut für Festkörpertheorie, Universität Münster, Wilhelm-Klemm-Straße 10, 48149 Münster

(Received 18 May 2001; published 15 November 2001)

In this work the complete valence-band structure of the molybdenum dichalcogenides MoS_2, $MoSe_2$, and α-$MoTe_2$ is presented and discussed in comparison. The valence bands have been studied using both angle-resolved photoelectron spectroscopy (ARPES) with synchrotron radiation, as well as *ab initio* band-structure calculations. The ARPES measurements have been carried out in the constant-final-state (CFS) mode. The results of the calculations show in general very good agreement with the experimentally determined valence-band structures allowing for a clear identification of the observed features. The dispersion of the valence bands as a function of the perpendicular component $\vec{k}_\perp$ of the wave vector reveals a decreasing three-dimensional character from MoS_2 to α-$MoTe_2$ which is attributed to an increasing interlayer distance in the three compounds. The effect of this $\vec{k}_\perp$ dispersion on the determination of the exact dispersion of the individual states as a function of $\vec{k}_\parallel$ is discussed. By performing ARPES in the CFS mode the $\vec{k}_\parallel$ component for off-normal emission spectra can be determined. The corresponding $\vec{k}_\perp$ value is obtained from the symmetry of the spectra along the ΓA, KH, and ML lines, respectively.

DOI: 10.1103/PhysRevB.64.235305 PACS number(s): 71.20.−b, 79.60.−i, 31.15.Ar

I. INTRODUCTION

The molybdenum dichalcogenides belong to the large family of layered transition metal dichalcogenides whose crystal structure results from the stacking of sheets of hexagonally packed atoms. It consists of weakly coupled sandwich layers X-Mo-X in which a Mo-atom layer is enclosed within two chalcogen layers (X=S, Se, Te). All three MoX_2 compounds crystallize in the $2H_b$ structure and MoS_2, as well as, $MoSe_2$ also crystallize in the 3R structure. In both of these polytype structures the coordination of the metal atoms is trigonal prismatic. In this work, $2H_b$ samples are investigated. For $MoTe_2$ a phase transition from the semiconducting $2H_b$-type α-$MoTe_2$ to a metallic polytype β-$MoTe_2$, with a monoclinic structure having a distorted octahedral coordination is known.[1–3] The $2H_b$ polytype, in the following assigned as $MoTe_2$, is stable below $\approx$815 °C.

The MoX_2 compounds are indirect semiconductors with indirect (direct) band gaps of 1.29 (1.78) eV for MoS_2, 1.10 (1.42) eV for $MoSe_2$, and 1.00 (1.10) eV for $MoTe_2$.[3] Since the optical band gaps are matching well with the solar spectrum these materials are used for electrodes in high efficiency photoelectrochemical (PEC) cells.[4] In the molybdenum dichalcogenides the phototransitions involve nonbonding d orbitals of Mo atoms. Therefore, these materials can be expected to resist hole-induced corrosion.[5] Despite of the major importance of the MoX_2 compounds in solar cell production, to date no comparative band structure determination from experiment and theory has been reported.

In general, it is expected that the gross features of the band structures of all three dichalcogenides are quite similar but, in addition, also some characteristic differences are to be expected. Several band structure calculations were performed so far which were used to explain experimental results from absorption measurements[6–9] and early photoemission work.[10–13] From the literature about these materials no consistent picture emerges (see, e.g., Ref. 14 for a review, and references therein). Therefore, we address in this work the electronic band structure of all three binary dichalcogenides on equal footing by ARPES measurements and by ''state-of-the-art'' *ab initio* band structure calculations. In experiment, high-resolution photoelectron spectrometers (with respect to emission angle and energy) are used. In addition, the constant-final-state (CFS) mode is applied to obtain data which shows low $\vec{k}_\perp$ dispersion. As to the theory, the electronic properties of all three molybdenum dichalcogenides are calculated within density functional theory (DFT) employing the local density approximation (LDA) (Ref. 15) and spin-orbit interaction is included. The present photoemission data and *ab initio* results constitute the first comprehensive picture of the electronic valence-band structure of all three molybdenum dichalcogenides.

II. CRYSTAL STRUCTURE

The $2H_b$-polytype of the crystal structure of the MoX_2 layer compounds is characterized by a stacking sequence /$AbABaB$/ (A, B: chalcogen atom layers; a, b: Mo atom layers).[16] A unit cell and the corresponding first Brillouin zone are displayed in Fig. 1. In this structure, a Mo atom layer is sandwiched between two chalcogen layers. The two X-Mo-X sandwich layers per unit cell are laterally displaced with respect to each other so that the Mo atoms of the upper sandwich layer are directly above the chalcogen atoms of the lower sandwich layer in the unit cell and vice versa. The sandwich layers are coupled only by weak van der Waals

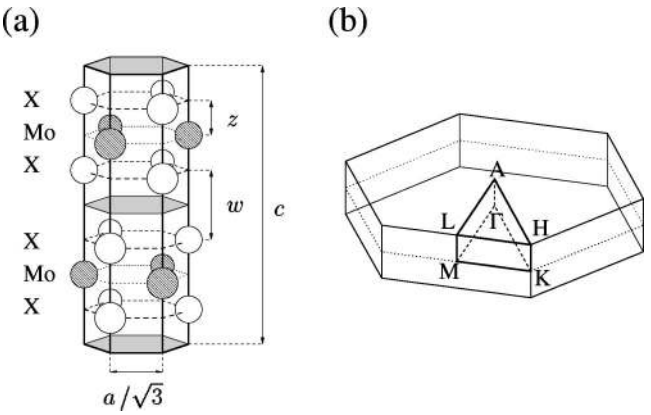

FIG. 1. Crystal structure (a) and the first Brillouin zone (b) of the $2H_b$ structure of the MoX_2.

forces giving rise to the quasi-two-dimensional character of the electronic structure.

The lattice parameters of the direct lattice a, c, w, and z are indicated in Fig. 1. In this work, we use averages of the a and c values, as reported in the literature from different experiments.[3,14,16] The thickness of a sandwich layer is taken to be $2z$ with $z=0.129c$. Therefore, an interlayer distance $w=c/2-2z=0.242c$ follows. In Table I the used average experimental structure parameters, the resulting c/a ratios, and the calculated reciprocal lengths of the most important high-symmetry lines [see Fig. 1 (b)] are given. In addition, the covalent radii of the chalcogen atoms and the ionic radii of the twofold negatively charged chalcogen ions are given. In the dichalcogenide crystals, the actual charge of the chalcogens is between the two limiting values of $0e$ and $-2e$ as a simple population analysis of the calulated density of states shows. It is obvious from Table I that the interlayer distance w, as well as, the lattice parameters a and c increase from MoS_2 to $MoTe_2$ mainly due to the increasing ionic radius of the chalcogen ions, while the c/a ratio remains nearly constant.

TABLE I. Structural parameters of the $2H_b$ polytype of the molybdenum dichalcogenides for the direct and reciprocal lattice. The parameter z, i.e., half the thickness of a sandwich layer, is given by $z=0.129c$. The size of the van der Waals gap w is calculated as $c/2-2z$. Furthermore the size of the Brillouin zone is determined by the respective $k_\parallel$ values. In addition, the covalent and ionic radii of the chalcogen atoms are given. The corresponding radii of molybdenum are Mo: 1.40 Å and Mo^{4+}: 0.70 Å, respectively.

	MoS_2	$MoSe_2$	$MoTe_2$
a[Å]	3.160	3.299	3.522
c[Å]	12.294	12.938	13.968
$2z$[Å]	3.172	3.338	3.604
w[Å]	2.975	3.131	3.380
c/a	3.891	3.922	3.966
$\overline{\Gamma A}$ [Å^{-1}]	0.255	0.243	0.225
$\overline{\Gamma M}$ [Å^{-1}]	1.148	1.099	1.030
$\overline{\Gamma K}$ [Å^{-1}]	1.325	1.270	1.189
$\overline{MK}$ [Å^{-1}]	0.662	0.636	0.594
r_{cov} [Å]	S: 1.04	Se: 1.17	Te: 1.37
r_{ion} [Å]	S^{2-}:1.84	Se^{2-}:1.98	Te^{2-}:2.21

III. EXPERIMENTAL APPROACH

A. Sample preparation and experimental setup

Naturally grown molybdenite (MoS_2) was used for this work. Excellent samples with sizes up to 3×3 mm^2 have been extracted from a larger piece. Single crystals of $MoSe_2$ and α-$MoTe_2$ were grown using the chemical vapor transport method (CVT) where bromine was used as the transport agent.

Coarse orientation of the samples was achieved by LEED patterns which were recorded under ultrahigh-vacuum conditions before cleavage. From the sharpness of the diffraction patterns it can be concluded that the single crystals are of high quality. Next, a small aluminum post was glued on top of the samples and they were inserted into the photoemission chamber. After preadjustment, the crystals were cleaved *in situ* by knocking off the aluminum posts. This was done at room temperature under ultrahigh-vacuum conditions ($p \leqslant 2\times10^{-10}$ mbar) to minimize surface degradation or contamination. Immediately after the cleavage a reference spectrum was recorded to check the surface quality from time to time. Even after up to fourty hours of data acquisition at room temperature no significant changes were observed. This is due to the crystals cleaving at the van der Waals gap resulting in a rather inert surface.

The measurements have been performed at the synchrotron radiation centers HASYLAB in Hamburg, Germany, and at BESSY-I in Berlin, Germany. The typical photon energy range of $h\nu=9\cdots30$ eV and a monochromator resolution of below 90 meV was used. The photoelectron spectrometers are hemispherical deflection analyzers mounted on two-axis goniometers. These are the WESPHOA-III station at the HONORMI beamline (W3.2) at HASYLAB and the new photoemission station AR 65 at the $3m$-NIM1 and $2m$-SEYA beamlines of BESSY-I.[17] For the measurements presented here, a monochromator resolution of 30–90 meV and an analyzer resolution of 50 meV were chosen, yielding an overall resolution of less than 100 meV. This is sufficient since all measurements were performed at room temperature. The maximum acceptance angle of the photoelectrons was $\approx\Delta\vartheta\pm0.8°$.

B. The CFS mode in photoemission

Photoemission spectroscopy can be performed in several different modes to determine the occupied bandstructure. Most common is the energy distribution curve (EDC) mode in which the photon energy is held constant and the detected kinetic energy is varied. With the emission angle ϑ (with respect to the surface normal) and the detected kinetic energy E_{kin} of the photoelectrons the wave-vector component parallel to the planes is determined by the dispersion relation

$$|\vec{k}_\parallel|=\frac{1}{\hbar}\sqrt{2m_eE_{kin}}\sin\vartheta. \quad (1)$$

The $\vec{k}_\perp$ component is not conserved since the electrons travel through the crystal surface. If the final state band can be approximated by a free electron parabola starting at the inner potential V_0, the following equation can be deduced:

$$|\vec{k}_\perp| = \frac{1}{\hbar}\sqrt{2m_e(E_{\mathrm{kin}}\cdot\cos^2\vartheta + V_0)}. \tag{2}$$

Obviously, $\vec{k}_\perp$ has to be larger than $(1/\hbar)\sqrt{2m_eV_0}$ in order to be able to observe photoemitted electrons outside the sample. A key question for the analysis of the experimental data is whether this approximation can be used for the molybdenum dichalcogenides in the final state energy range used in this work. Recently Strocov *et al.*[18,19] have claimed that this approximation might not be suitable for two-dimensional layered transition-metal dichalcogenides. We will come back to this point in Sec. V A. In addition, Strocov *et al.* found for TiS_2 and VSe_2 that the inner potential V_0 is dependent on $\vec{k}$ for these materials. In the present study of the molybdenum dichalcogenides, V_0 has been determined by LEED-I/V curves where intial electron energies between 50–250 eV have been used. For V_0 we have determined 12.0 ± 2.3 eV in MoS_2, 14.5 ± 1.5 eV in $MoSe_2$ and 16.1 ± 1 eV in $MoTe_2$. An error of about 1.5 eV can be assumed for the determination of V_0 by the LEED-I/V curve technique. Larger errors result from the statistical spread over several samples which have been investigated. For normal emission the critical points can be found accurately from the symmetry of the dispersion of the uppermost band along $\overline{\Gamma A\Gamma}$. By this procedure the experimental band structure at the high symmetry points can directly be compared to the corresponding calculated band structure.

The constant-final-state mode has some advantages with respect to the EDC mode. For example, Eqs. (1) and (2) show that both $\vec{k}$ components depend on the kinetic energy. Therefore, the emission features in an EDC spectrum are affected by a dispersion in both directions. For a strongly dispersing band the corresponding peaks are asymmetric within the EDC spectra. This can be avoided in the CFS mode, where both $\vec{k}$ components ($\vec{k}_\parallel$ and $\vec{k}_\perp$) are kept constant. A spectrum at a new value of, e.g., $\vec{k}_\parallel$ is adjusted by choosing a couple $(E_{\mathrm{kin}},\vartheta)$ for which $\vec{k}_\perp$ remains constant. The range of these values is limited by the monochromator energy range so that not all high-symmetry directions are accessible. Another advantage of the CFS mode lies in the fact that the detected kinetic energy at the analyzer is kept constant, too. Since the transmission function increases for lower E_{kin} values an EDC spectrum typically reveals an increased background towards the low energy region, which cannot be determined exactly. In the CFS mode, only the characteristics of the monochromator (i.e., photon flux per photon energy) influences the background of each spectrum. But this can be determined exactly, e.g., by measuring the current of a reference gold mesh which is positioned in the photon beam.

C. Data analysis technique

Each spectrum measured in the present work has been modeled by a curve fitting program based on the Levenberg-Marquardt algorithm.[20] The model function is created by convoluting a sum of peaks plus Shirley-background[21] with the Gaussian shaped spectrometer function. Many emission features with larger binding energy reveal a Lorentzian line shape which is in agreement with the physical nature of the electronic states. A typical full width at half maximum of 200–400 meV indicates that the intrinsic line shape cannot be influenced by the spectrometer function since the latter was always chosen to be lower than 100 meV in width (i.e., analyzer plus monochromator resolution). Since in the CFS mode the whole spectrum belongs to one specific $\vec{k}$ vector, the line shape cannot be influenced by dispersion effects which may occur in EDC spectra.

IV. BAND-STRUCTURE CALCULATIONS

The LDA-DFT calculations have been carried out employing the norm-conserving, nonlocal pseudopotentials of Bachelet, Hamann, and Schlüter.[22] The exchange-correlation energy was taken into account using the Ceperley-Alder[23] form as parametrized by Perdew and Zunger.[24] As a basis to represent the wavefunctions, we use 120 Gaussian orbitals of s, p, d, and s^* symmetry per sandwich layer and spin. At each atomic position, 40 orbitals are localized. The decay constants of the Gaussians employed are {0.17,0.45,1.18,2.00} for Mo, {0.17,0.45,0.90,1.70} for S, {0.17,0.45,0.90,1.80} for Se, and {0.17,0.43,1.05,2.60} for Te (in atomic units). A real space mesh with linear spacings of about 0.2 Å is used for the representation of the charge density and the potential. The spin-orbit interaction is treated in an on-site approximation, i.e., only integrals with the same location of the Gaussian orbitals and the spin-orbit potential are taken into account. Brillouin-zone integrations have been carried out using 12 special **k** points in the irreducible part of the Brillouin zone.

In our calculations we find, that a number of electronic features depend sensitively on the lattice parameters. Therefore, we have used in the calculations reported in this work a value of $z=0.129c$ for half the diameter of the sandwich layers as obtained in experiment in order to arrive at a more meaningful comparison between theoretical and experimental results. Our calculations of z by total energy minimization (with a and c being held constant) yield $0.125c$ for MoS_2, $0.128c$ for $MoSe_2$, and $0.127c$ for $MoTe_2$, i.e., values which are somewhat lower than the experimental values.

V. RESULTS AND DISCUSSION

A. Final states

As mentioned above, the knowledge of the final state and the corresponding $\vec{k}_\perp$ component is very important when the CFS mode is applied in photoemission. Equation (2) assumes free-electron-like final-state bands which in general, as claimed by Strocov *et al.*,[18] might not be a good approximation for layered transition-metal dichalcogenides. As a result

from their study of TiS_2 and VSe_2, the authors argued that the complicated dispersion of the final state bands affects the band mapping in a way that the $\vec{k}_\perp$ component remains undetermined. In contrast, it can be expected for quasi-two-dimensional materials and especially for the MoX_2 compounds that the $E(\vec{k}_\perp)$ dependence is significantly smaller than the $E(\vec{k}_\parallel)$ dependence.

To determine experimentally the critical points at the zone edge a number of CFS spectra have been recorded. In particular, CFS spectra with $\vec{k}_\parallel$ vectors along the ΓK direction at four different $\vec{k}_\perp$ values corresponding to (0.0 π/c, -0.25 π/c, 0.50 π/c, and 1.0 π/c) were recorded and analyzed. The first of these four values corresponds to spectra taken along the ΓK and the last along the AH direction in the Brillouin zone. The experiments were carried out for MoS_2 at the HONORMI beamline in HASYLAB (DESY, Hamburg) where a photon energy range of $h\nu = 10$–30 eV can be used. MoS_2 was chosen since this material is expected to reveal the most pronounced three-dimensional character in the band structure. Nevertheless, the respective dispersion in most cases was found to be very small, as compared to the dispersion of the bands along the $\vec{k}_\parallel$ in-plane directions. Within the available photon energy range it was possible to record CFS series along the ΓK (AH) directions at four different $\vec{k}_\perp$ values.

Figure 2 presents the experimental band-structure features as resulting for $E(\vec{k}_\parallel;\vec{k}_\perp$ fixed) with the four different $\vec{k}_\perp$ values noted above and indicated in the figure. For the sake of clarity only pronounced emission features in the spectra are shown in the figure. The filled circles mark the ΓK direction with the $\vec{k}_\perp$ value of the Γ point. In general, the symbols of the other three series of measured features for the other three $\vec{k}_\perp$ values lie very close to the circles. This is especially striking for the upper bands near K/H. Only the two uppermost measured bands near Γ/A show a significant dependence on the $\vec{k}_\perp$ value. Also the bands between -2.0 and -6 eV do not reveal a very pronounced $E(\vec{k}_\perp)$ dependence.

At this point it is very revealing to compare some of the above discussed experimental results with results of our band-structure calculations. A respective comparison for $\vec{k}_\perp$ equivalent to zero, i.e., along the ΓK direction is shown in Fig. 3. An amazingly good agreement between theory and experiment for most of the bands is obvious in Fig. 3 lending further support to the accurate experimental determination of the high symmetry line. Most of the Mo $4d$ and S $3p$-derived bands between 0 and -5 eV are found to be in very good agreement. Only the S $3p$-derived band around -6 eV shows significant deviations. One possible origin of this behavior in experiment could be the large width in the underlying data, especially at Γ, so that the assignment of the measured structures to a well-defined binding energy is difficult. Another origin of the seeming disagreement could be related to the symmetry dependence of the observed spectral features. We come back to this point in Sec. V B. The band in question originates from sulfur $3p$ valence states and its dispersion is determined by the interaction of these states across the van der Waals gap.

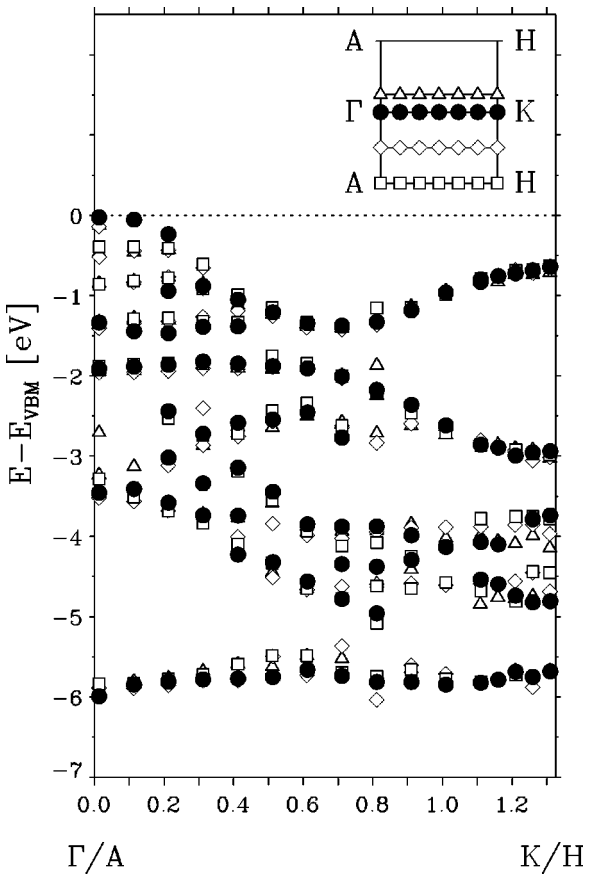

FIG. 2. The experimentally derived band structure of MoS_2 along the ΓK and AH, as well as, two other parallel lines as indicated in the inset.

To obtain further evidence that the K and the M point at the zone edge can be accurately determined, CFS series along the KH and ML high-symmetry lines were recorded. The respective $\vec{k}_\perp$ values have been calculated by using Eq. (2) even if this approximation is quite coarse. This is sufficient since the determination of the critical points has been done experimentally. In this case, $MoSe_2$ was chosen as the example since it shows a distinct spin-orbit splitting along the KH line in addition to a clear three-dimensional band character. After analyzing the spectra by the curve fitting approach discussed above, a weak $E(\vec{k}_\perp)$ dependence is observed in the data.

This is shown in Fig. 4 where the experimental data are compared to the corresponding calculated bands. The energy axis is aligned to the valence-band maximum which results from further investigations presented in the next sections. First we note that there is a reasonable general correspondence between the number and energy position of measured and calculated bands. Even the dispersion of the theoretical and experimental results show good agreement in cases. The absolute binding energy for the topmost emission features, however, are slightly lower than the energies of the respective calculated bands. One can therefore conclude from the

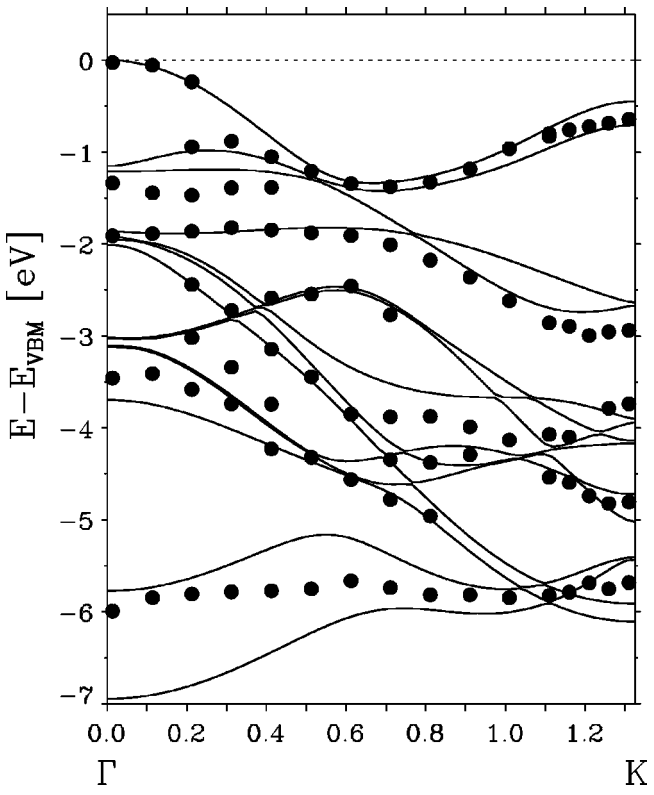

FIG. 3. Experimentally derived band structure (symbols) of MoS_2 along the ΓK line in comparison with the respective calculated bulk band structure (solid lines).

dispersion and energy position of the topmost bands and from the bands in the energy region around -2.5 eV that the K and the M points can be determined. By having the three high symmetry points, namely, Γ, K, and M, one is able to scan all high-symmetry lines.

Despite a good correspondence of the states with smaller binding energies up to -3.0 eV the states between -3.5 and -4.5 eV along the KH symmetry line show a fairly

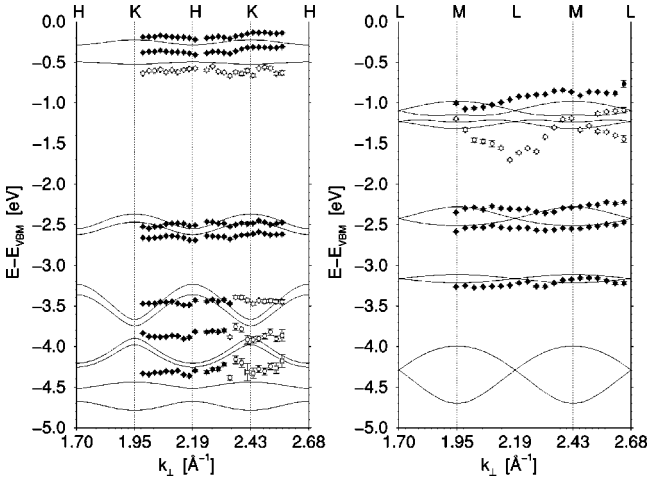

FIG. 4. Experimental valence-band structure (symbols) of $MoSe_2$ along the symmetry lines KH and ML in comparison with the calculated bands (solid lines).

poor agreement with theory. In particular, the calculated bands show a significant $\vec{k}_\perp$ dispersion while experiment observes nearly dispersionless states. We have observed the same behavior already in Fig. 3, where two bulk bands at about -6 and -7 eV were found while experiment observed only one very narrow band. We come back to this point further below. For the ML direction a direct comparison of the bands in the latter energy region is not possible, since the respective bands could not be observed in experiment because of the limited monochromator energy range.

B. Valence-band structure along ΓA

Normal emission spectra for all three materials were recorded at various beamlines at HASYLAB or BESSY-I synchrotron sources, respectively, in the energy range of 13–30 eV. The energy axis is referred to the valence-band maximum which was determined in connection with the complete valence-band structure as described in the following sections. To determine the band structure from the spectra series all spectra were modeled after the removal of a small Shirley background[21] by a sum of Gaussian and Lorentzian profiles. The $\vec{k}_\perp$ value within the Brillouin zone to which each peak has to be attributed was calculated from Eq. (2). As pointed out above, in this limited energy range of about 10–30 eV this equation can be used allowing for a sufficiently precise calculation of the $\vec{k}_\perp$ value for each energetic peak position. For larger energies the deviation of the final states from free-electron-like behavior must be taken into account. Here target current spectroscopy might be applied to first determine the coupling bands and then measure all photoemission spectra in the CFS mode with the final state belonging to the specific coupling band.[19,25,26]

Before addressing the observed band structures along ΓA in detail we note that only each second Γ point is observed in experiment. According to Ref. 27 this is due to the fact that in nonsymmorphic crystal structures the symmetry of the final state is not always unique as it is for symmorphic structures. The ΓA direction Δ consists of the points $\vec{k} = 2\pi/c(0,0,\delta)$ with $0<\delta<\frac{1}{2}$. Δ represents a group with a number of operations which are listed for instance in the above reference. For example a plane wave of the form $\exp[i2\pi/c(0,0,\delta)(x,y,z)]$ is transformed by any operation from Δ to an irreducible representation and this plane wave belongs to, e.g., Δ_1. In contrast a plane wave $\exp[i2\pi/c(0,0,\delta+1)(x,y,z)]$ which is streched by a reciprocal lattice vector $2\pi/c(0,0,1)$ belongs to Δ_2. Obviously the symmetry depends on the length of the wave vector. For a given final state symmetry this leads to the observed missing of each second Γ point since each second initial state reveals an odd symmetry. This fact has to be taken into account in the comparison to the band structure calculations.

The experimental band structures along $\overline{\Gamma A \Gamma}$ are shown in Figs. 5, 6, and 7 together with the results of our band structure calculations. In one case (Fig. 5) we have included the density of states of the bands along the ΓA direction, as well. We first address the experimental results. In general, for all three materials one can easily distinguish at least two

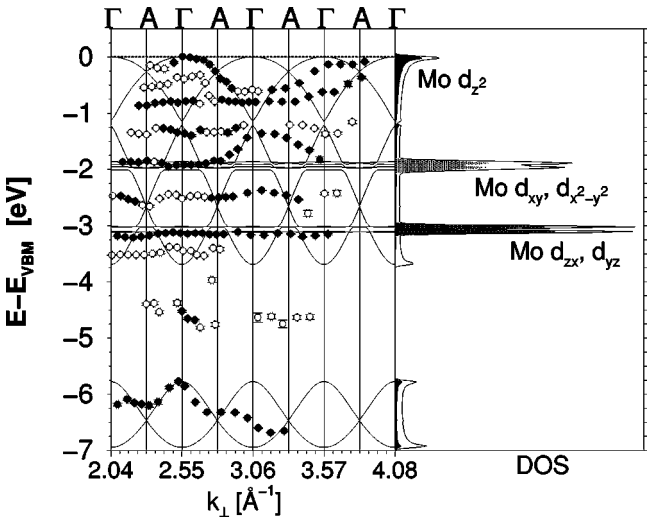

FIG. 5. Experimental valence-band structure (symbols) of MoS_2 along the ΓA high-symmetry line in comparison with the calculated band structure (solid lines). Open symbols denote weak measured structures. The error bars are due to the limited experimental energy and angular resolution and due to uncertainties from the curve fitting. In addition, the density of states for the bands along ΓA is plotted. The contributions of particular molybdenum *d*-states is indicated by the shaded regions.

dispersive structures and a number of nearly nondispersive bands. The uppermost valence band, as well as, the band with the largest binding energy reveal a significant $\vec{k}_\perp$ dependence. The width of the uppermost band between Γ and A decreases from MoS_2 to $MoTe_2$, i.e., the bands become more two-dimensional and less $\vec{k}_\perp$ dependent. This effect is not so strong for the band with the largest binding energy but also noticeable. From this result one may conclude that the latter might be predominantly of chalcogen p_z orbital character, which is relatively strongly influenced by the following sandwich layer in the crystal. Indeed, our band structure calculations exhibit a contribution of the chalcogen p_z orbitals from 66 to 60 % for the three chalcogenides to this state. In contrast, the influence of the next sandwich layer on the predominantly Mo $4d_{z^2}$-derived states (61 to 68 % metal d_{z^2} character) at the valence-band maximum decreases rapidly with the increasing size of the unit cell.

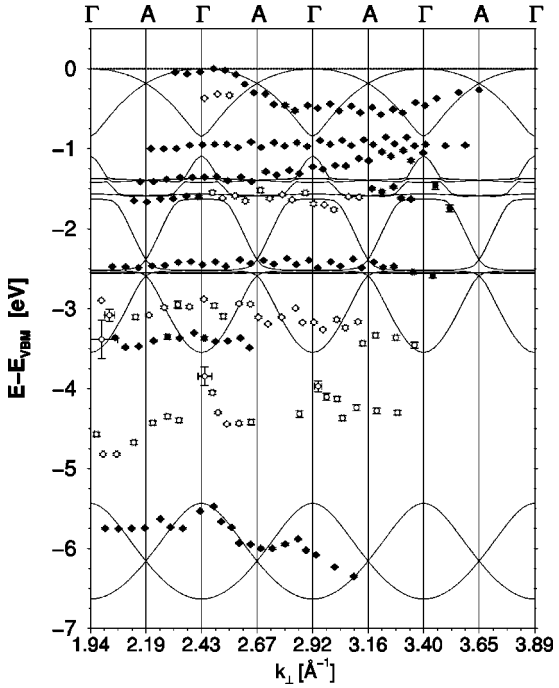

FIG. 6. Experimental valence-band structure (symbols) of $MoSe_2$ along the ΓA high-symmetry line in comparison with the calculated band structure (solid lines). Open symbols denote weak structures. The error bars are due to the limited experimental energy and angular resolution and due to uncertainties from the curve fitting.

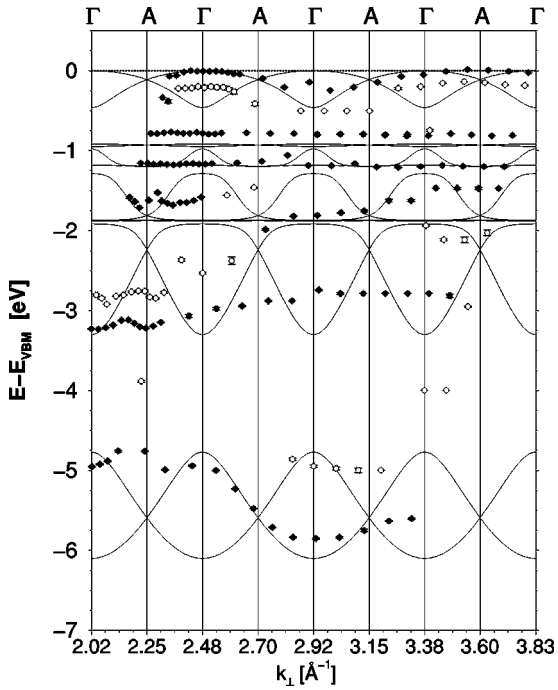

FIG. 7. Experimental valence-band structure (symbols) of $MoTe_2$ along the ΓA high-symmetry line in comparison with the calculated band structure (solid lines). Open symbols denote weak structures. The error bars are due to the limited experimental energy and angular resolution and due to uncertainties from the curve fitting.

It should be noted that in all compounds the topmost band at the second Γ point (for which it can be observed) lies at larger binding energies in comparison to the first one. This may be attributed to two effects. First, the analyzer has a fixed maximum acceptance angle $\vartheta_{\max}$. The $\vec{k}$ resolution Δk depends on this acceptance angle and on the kinetic energy [see Eq. (1)]. Assuming $\vartheta_{\max}=0.8°$ then for the first Γ point $\Delta k \approx 0.020$ [Å^{-1}] while for the second one it is $\Delta k \approx 0.036$ [Å^{-1}]. Since the Γ point is the point with the highest symmetry the band disperses in all $\vec{k}$ directions away from Γ to larger binding energies. For a lower $\vec{k}$ resolution the band position at all $\vec{k}$ values within this range must be integrated. This yields an emission feature with a maximum at a larger binding energy. The second effect might be the

reduced information depth at higher photon energies. If the mean free path becomes lower than one unit cell, the $\vec{k}_\perp$ dependence will smear out and the spectra will reflect a more one-dimensional density of states.[28]

Below the two dispersive bands a number of nearly perfect dispersionless bands are observed. The density of states resolved with respect to Mo $4d$ and S $3p$ character in Fig. 5 clearly reveals the physical origin of some of these features. From the results of our band-structure calculations it is most obvious, that these bands are two-dimensional and can be attributed to Mo $4d$ states (see the calculated density of states in Fig. 5 for that matter). In the calculations, they are located at about -1.8 and -3.1 eV and the bands are separated in both cases due to spin-orbit interaction. For MoS_2 this splitting is too small to be observed in experiment. In contrast, for the other two compounds the photoemission data clearly exhibit the splitting of the dispersionless bands at about -1.5 and -1.1 eV, respectively. In $MoSe_2$ this energetic separation is about 300 meV and for $MoTe_2$ it is about 500 meV. So, the energetic separation of these two spin-orbit splitted band groups, as well as, their binding energy decrease towards the tellurium compound in very good agreement between theory and experiment. The density of states in the other energy regions (see Fig. 5) is comparatively small, so that respective band-structure features are more complicated to measure.

Thus a comparison with the calculated band structures in general shows very good agreement, indeed, in spite of the fact that some experimentally observed emission features do not result from the calculations. In all three compounds such emissions are found above the lowest binding energy state at about -4.5 eV. Typically this is only a very weak structure but it is also directly visible in the spectra of, e.g., MoS_2 in the energy range of 21–23 eV. Additional states may also arise from transitions of an initial state to a neighboring final state with different binding energy. Since an energy distribution curve provides only combined information of the initial, as well as, the final state it cannot be distinguished between such effects. Of course, one would expect that only one coupling band is suitable for a given initial state but as it has been stated by Strocov *et al.*,[18] in some cases an additional final state branch may exist. The emission intensity is then expected to be lower as from the main branch and this can be supported by the observed features in the present spectra.

Additional valence bands between the nondispersive bands and the topmost valence band are experimentally observed but not supported by theory. A number of the respective spectral features are quite intense and might not be explained by different coupling branches. In MoS_2 at least two strong emission features appear at about -1.3 and -0.8 eV which are quite nondispersive for lower photon energies. For higher photon energies, i.e., beyond the second Γ point the band near -0.8 eV begins to disperse to smaller binding energies while the band which is found energetically below the former vanishes.

Finally, we note that all three valence band structures in Figs. 5, 6, and 7 show valence bands within the energy region from -5–7 eV with significant $\vec{k}_\perp$ dispersion. This dispersion shows the symmetry properties, as discussed above, in that only one of the two bands between consecutive Γ points is seen in experiment. The agreement between the respective theoretical and experimental bands is particularly close for $MoTe_2$ as can be seen in Fig. 7. By the same token, it becomes most obvious, why experiment observes in this energy region for one particular Γ point either the upper or the lower band but not both. Since the experimental data plotted in Fig. 3 were recorded for one particular $\vec{k}_\perp$ at the Γ point only one band could be observed.

C. Valence-band structure along the in-plane directions

After the discussion of the valence-band structure in the ΓA direction we now focus on the directions parallel to the layers. We discuss the band structures along the high-symmetry lines ΓK, ΓM, and MK of the Brillouin zone. The ΓK direction is the longest high-symmetry line. In the case of the molybdenum dichalcogenides this direction is most important since the energetic position of the topmost emission features at the Γ and the K point determine a number of electrical and optical properties.

Figure 8 shows CFS spectra for the three molybdenum dichalcogenides recorded along the ΓK line. The respective final state was chosen such that $\vec{k}_\perp$ remains in the ΓKM plane within the whole series of spectra. Here the experimental determination of the Γ, K, and M point has been taken into account.

A number of features is easily recognized in the spectra of Fig. 8. The three series reveal a close similarity of the $E(\vec{k})$ behavior of most emission features. Starting at Γ (i.e., $k_\parallel = 0.0$ Å^{-1}) to the K point the states near -3.2 eV and the lowest binding energy disperse towards larger binding energies. This is different from the two topmost emission features, which separate from each other after nearly halfway towards K and move with nearly constant width to K.

From the spectra in Fig. 8 it can be deduced that for MoS_2 the topmost emission feature near Γ reveals the weakest intensity compared to the other compounds. Since this state is predominantly derived from the Mo $4d_{z^2}$ orbitals (see previous section) high spectral intensity for this state is expected. It should be decreased for a lower lattice parameter a due to a shielding by the chalcogen p orbitals. Indeed this is observed. Furthermore, the topmost emission feature reveals a decreasing dispersion from MoS_2 to $MoTe_2$.

The spectra for the ΓK and ΓM directions are largely similar. The spectra along the MK direction show relatively small dispersions, as compared to those along ΓK and ΓM. Only the features with the smallest binding energy show appreciable dispersion.

D. The spin-orbit splitting at *K*

Before discussing the complete valence-band structure of the three molybdenum dichalcogenides, we first briefly address the effects of spin-orbit coupling on the spectra and the band structures. A distinct splitting of the emission features with lowest binding energy at the K point can be observed in Fig. 8. It is most obvious for $MoTe_2$ and is only visible as a

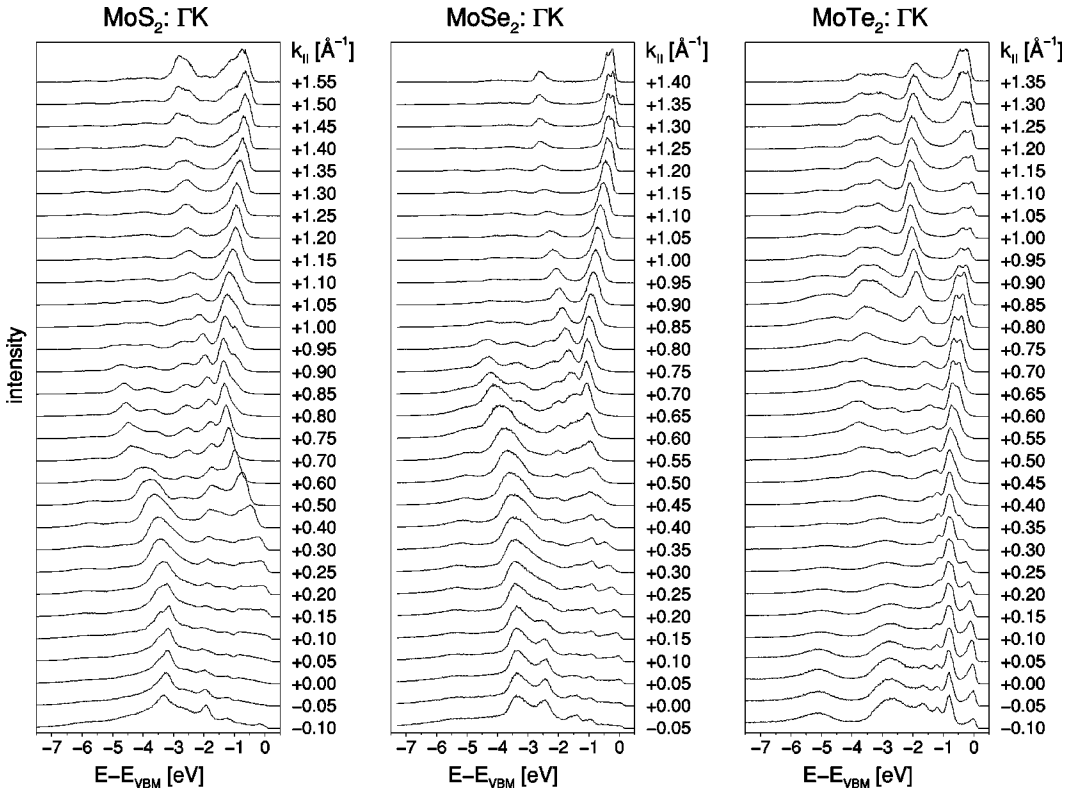

FIG. 8. ARPES spectra recorded in the CFS mode along the high-symmetry line ΓK of the three molybdenum dichalcogenide compounds. The size of $k_{\parallel}$ at the K point is given in Table I.

weak shoulder in the MoS_2 compound. Figure 9 shows the relevant part of the spectra for each compound where the double emission feature is assigned with X and Y, respectively, in line with previous work on $MoTe_2$.[29] A broad additional emission feature denoted as "add." is taken into account which is present in all three spectra just below peak X.

The size of the splitting of these bands at the K point in the experimental spectra and in the theoretical results is listed in Table II. From MoS_2 to $MoTe_2$, the splitting increases with increasing Mo d character of the bands. Furthermore, the energetic position of the bands move towards the valence-band maximum at the Γ point (see Fig. 9).

The general trend in the observed energetic differences whithin the row of the three dichalcogenides is observed in the theoretical results, as well. The experimentally observed splittings of the emission features X and Y at the K point, however, are about 100 meV smaller than the respective calculated splittings.

Another point concerning the splitting at K is connected with the interpretation of two structures in optical measurements. Optical absorption spectra of all three MoX_2 compounds display excitonic features characteristic of the group VIA transition metal dichalcogenides.[6,30] As claimed by Coehoorn *et al.*,[11] who observed a splitting of 0.21 eV for $MoSe_2$ at the K point, these states give rise to the so-called A and B excitons. The splitting found in Ref. 11 for $MoSe_2$ matches well with the observed energetic difference of the A and B excitons (see, e.g., Ref. 31) and therefore the authors concluded that probably the exciton peaks arise from the two possible transitions at the K point.

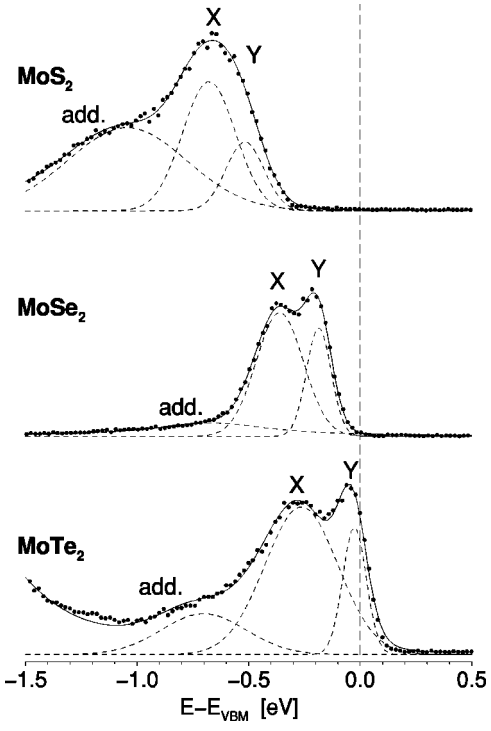

FIG. 9. Double emission feature for the three dichalcogenides at the K point. Filled circles denote the experimental data while the solid lines represents the fit curve as obtained from the sum of two Gaussians (dashed lines) (X,Y) and an additional weak emission feature labeled "add."

TABLE II. Energetic separation of the emission features *X* and *Y* at the *K* point in comparison with the calculated splitting. The right column gives the energetic distance between the *A* and *B* excitons following from optical absorption measurements (Ref. 6).

	Splitting at K		*A*, *B* excitons
	Exp. ARPES data	Calculation	Exp. opt. data
MoS_2	161±10 meV	258 meV	180 meV
$MoSe_2$	175±10 meV	294 meV	250 meV
$MoTe_2$	238±10 meV	331 meV	380 meV

Additionly, Finteis *et al.* found the valence-band maximum of WSe_2 to be located at the *K* point in their experiments.[28,32] The latter authors also concluded that the double emission feature at the *K* point is the signature of the two initial states of the excitons *A* and *B*. To attribute the double emission feature at the *K* point to the initial states of the excitons *A* and *B* is at variance, however, with several investigations using optical absorption measurements[6,7,33] leading to the result that appropriate transitions for the *A* and *B* excitons should occur at the Γ point. However, according to the present experimental data the peak distances as listed in Table II for the double feature *X*, *Y* for all three materials are too small compared to the energetic distance of the excitonic lines measured by, e.g., Beal *et al.*[6] Even though a shift between the initial states and the observed energy distance of the excitons is possible[34] the magnitude of the observed shift cannot be explained within the theory.[34] It must be concluded accordingly that the double emission feature *X*, *Y* at the *K* point does not correspond to initial states of the excitons *A* and *B*.[29] In line with the optical absorption measurements cited above and from the location of the VBM at the Γ point it is suggested that the topmost occupied state at Γ is the initial state for the *A* and *B* excitons.

E. Complete valence-band structures

In Figs. 10, 11, and 12 the experimentally observed spectral features (see Sec. V C) of each molybdenum dichalcogenide compound are plotted as a band structure along the high-symmetry lines $M\Gamma KM$ in direct comparison with the results of our band-structure calculations. A projected band structure has not been used since the respective critical points have been determined experimentally.

The lower unoccupied bands are also shown. Except for the gap problem within the LDA the dispersion of these bands should be correct. The comparison with the results of inverse photoemission investigations on MoS_2 (Refs. 35,36) confirms this finding. Also studies on the similar material WSe_2 show good qualitative agreement.[37] Thus it can be concluded that the minimum of the conduction bands is located nearly halfway between Γ and *K*, indeed. Furthermore, the valence-band maximum is found at Γ in all three compounds. This is confirmed for all three materials by the experimental data. From the present band structure calculations it follows that the energetically lowest indirect transition is from Γ to $\approx\frac{1}{2}\Gamma K$ and the lowest direct transition occurs at *K*.

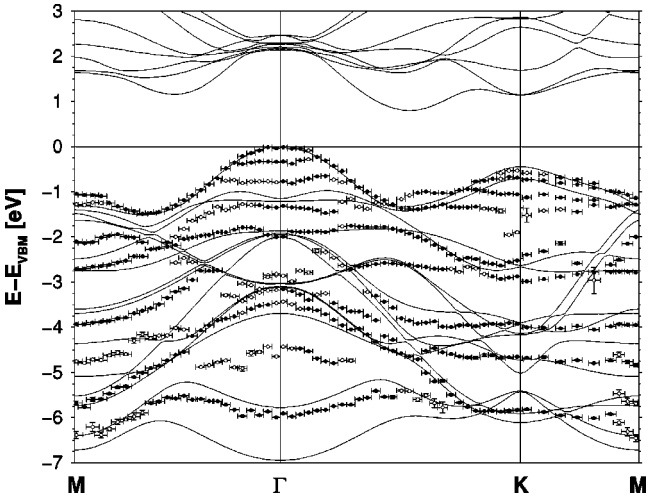

FIG. 10. Experimental valence-band structure (symbols) of MoS_2 along the in-plane directions $M\Gamma$, ΓK, and KM in comparison with the calculated band structure (solid lines). Open symbols denote weak structures. The error bars are due to the limited experimental energy and angular resolution and due to uncertainties from the curve fitting.

A close look at the valence-band structure of all three materials reveals a very good general agreement between measured and calculated bands. The total valence-band width is found to decrease from MoS_2 over $MoSe_2$ to $MoTe_2$ both in experiment and theory.

The dispersion of the uppermost bands away from Γ towards *K* and *M* reveal also quantitative matching. However, the energetic positions of the calculated bands in the vicinity of the high-symmetry point *K* differ with a maximum difference of 200 meV in the case of $MoSe_2$. Also the calculated splitting of the bands at *K* (already discussed above) is about 100 meV larger than observed in experiment. The general

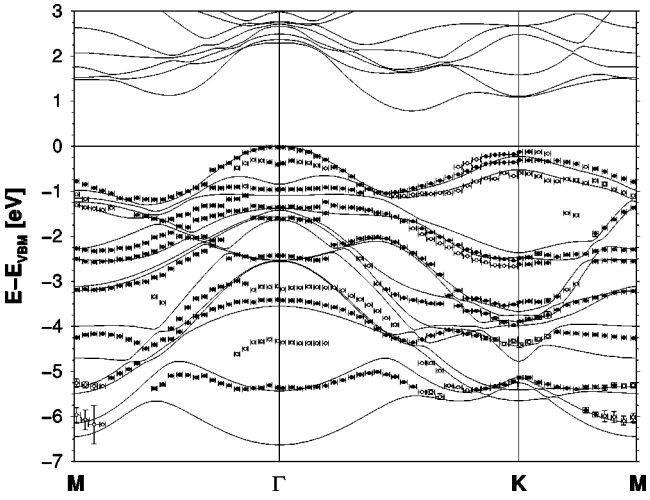

FIG. 11. Experimental valence-band structure (symbols) of $MoSe_2$ along the in-plane directions $M\Gamma$, ΓK, and KM in comparison with the calculated band structure (solid lines). Open symbols denote weak structures. The error bars are due to the limited experimental energy and angular resolution and due to uncertainties from the curve fitting.

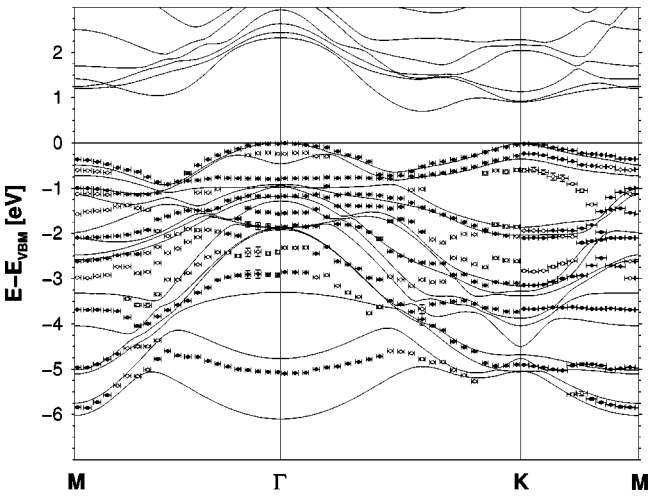

FIG. 12. Experimental valence-band structure (symbols) of $MoTe_2$ along the in-plane directions $M\Gamma$, ΓK, and KM in comparison with the calculated band structure (solid lines). Open symbols denote weak structures. The error bars are due to the limited experimental energy and angular resolution and due to uncertainties from the curve fitting.

trend in decreasing binding energy of the top of the valence bands at M, as observed in experiment, results from theory, as well. Only the absolute energetic location of the topmost state at M is about 200 meV too low as compared to the photoemission results. It must be emphasized that such differences between experiment and theory in the range of a few 100 meV are close to the theoretical uncertainty that can be achieved nowadays.

In the vicinity of about -1 eV a dispersionless band is observed in the ΓA direction (see Figs. 5, 6, and 7) which is also dispersionless near the center of the Brillouin zone for off-normal emission (see Figs. 10, 11, and 12).[38–40] In the ΓKM plane, this band is found experimentally in MoS_2 to be ≈ 100 meV below a rather dispersionless band in the calculated band structure and about 100 meV above the respective band for $MoSe_2$ and $MoTe_2$. On the other hand, along ΓA only in the case of $MoTe_2$ this band results from the theory.

In band structure calculations for the (0001) surface of MoX_2 (X=S, Se, Te), which we have carried out using a slab of 9 sandwich layers (method as described in Ref. 37), we have found states located at the first few sandwich layers of the surface in this energy range. The respective bands exhibit only a small dispersion around the center of the surface Brillouin zone in agreement with the experimentally observed bands. Therefore, one might attribute these bands in the photoemission data to surface states.

VI. CONCLUSIONS

In our investigations, we have determined the complete valence-band structure of MoS_2, $MoSe_2$, and α-$MoTe_2$ on equal footing by experiment and theory. It was found that the valence bands resulting from angle-resolved photoelectron spectroscopy in the constant-final-state mode and from *ab initio* calculations are in very good overall agreement. Our results yield the first comprehensive picture of the electronic bulk valence-band structure of all three molybdenum dichalcogenides.

ACKNOWLEDGMENTS

We would like to thank D. Kaiser for natural MoS_2 samples, A. Klein from Technische Universität Darmstadt for the $MoSe_2$ samples, and D. Kaiser and J. Augustin for the $MoTe_2$ samples. This work received funding from the Bundesministerium für Bildung, Wissenschaft, Forschung und Technologie (BMBF) under Project No. 05 622 KHA and No. 05 SE8 PMA 6.

[1] R.M.A. Lieth and J.C.J.M. Terhell, in *Preparation and Crystal Growth of Materials with Layered Structures*, edited by R.M.A. Lieth (Reidel, Dordrecht, 1977), p. 141.

[2] S.W. Hla, V. Marikovi ć, A. Prodan, and I. Muševič, Surf. Sci. **352-354**, 105 (1996).

[3] Gmelin, in *Gmelin Handbook of Inorganic and Organometallic Chemsitry* (Springer-Verlag, Berlin, 1995), Chap. Mo Suppl. Vol. B 7,8,9, p. 16.

[4] H.D. Abruña, G.A. Hope, and A.J. Bard, J. Electrochem. Soc. **129**, 2224 (1982).

[5] M. Kettaf, A. Conan, A. Bonnet, and J.C. Bernede, J. Phys. Chem. Solids **51**, 333 (1990).

[6] A.R. Beal, J.C. Knights, and W.Y. Liang, J. Phys. C **5**, 3540 (1972).

[7] R.A. Bromley, R.B. Murray, and A.D. Yoffe, J. Phys. C **5**, 759 (1972).

[8] B. L. Evans, in *Physics and Chemistry of Materials with Layered Structures* (Lee, Eindhoven, NL, 1976), Chap. Optical Properties of layered Compounds, pp. 103–143.

[9] W.Y. Liang, J. Phys. C **6**, 551 (1973).

[10] R. Coehoorn, C. Haas, J. Dijkstra, C.J.F. Flipse, R.A. de Groot, and A. Wold, Phys. Rev. B **35**, 6195 (1987).

[11] R. Coehoorn, C. Haas, and R.A. de Groot, Phys. Rev. B **35**, 6203 (1987).

[12] R. Mamy, A. Boufelja, and B. Carricaburu, Phys. Status Solidi B **141**, 467 (1987).

[13] K. Fives, I.T. McGovern, R. McGrath, R. Cimino, G. Hughes, A. McKinley, and G. Thornton, J. Phys.: Condens. Matter **4**, 5639 (1992).

[14] R. Manzke and M. Skibowski, in *Landolt-Börnstein/New Series III 23 B: Electronic Structure of Solids: Photoemission Spectra and Related Data*, Group iii, edited by A. Goldmann (Springer-Verlag, Berlin, 1994), Vol. 23 (Subvol. B), Chap. 2.7.3 VIB-VIA-compounds, p. 131.

[15] P. Hohenberg and W. Kohn, Phys. Rev. **136**, B864 (1964).

[16] J.A. Wilson and A.D. Yoffe, Adv. Phys. **18**, 193 (1969).

[17] C. Janowitz, R. Müller, T. Plake, Th. Böker, and R. Manzke J. Electron Spectrosc. Relat. Phenom. **105**, 43 (1999).

[18] V.N. Strocov, H.I. Starnberg, P.O. Nilsson, H.E. Brauer, and L.J. Holleboom, J. Phys.: Condens. Matter **10**, 5749 (1998).
[19] V.N. Strocov, H.I. Starnberg, and P.O. Nilsson, J. Phys.: Condens. Matter **8**, 7539 (1996).
[20] W.H. Press, S.A. Teukolsky, W.T. Vetterling, and B.P. Flannery, *Numerical Recipes in C* (Press Syndicate of the University of Cambridge, Cambridge, 1992).
[21] D.A. Shirley, Phys. Rev. B **5**, 4709 (1972).
[22] G.B. Bachelet, D.R. Hamann, and M. Schlüter, Phys. Rev. B **26**, 4199 (1982).
[23] D.M. Ceperley and B.J. Alder, Phys. Rev. Lett. **45**, 566 (1980).
[24] J.P. Perdew and A. Zunger, Phys. Rev. B **23**, 5048 (1981).
[25] V.N. Strocov, Int. J. Mod. Phys. B **9**, 1755 (1995).
[26] V.N. Strocov, H.I. Starnberg, P.O. Nilsson, and L.J. Holleboom, J. Phys.: Condens. Matter **8**, 7549 (1996).
[27] D. Pescia, A.R. Law, M.T. Johnson, and H.P. Hughes, Solid State Commun. **56**, 809 (1985).
[28] Th. Finteis, M. Hengsberger, Th. Straub, K. Fauth, R. Claessen, P. Auer, P. Steiner, S. Hüfner, P. Blaha, M. Vögt, M. Lux-Steiner, and E. Bucher, Phys. Rev. B **55**, 10 400 (1997).
[29] Th. Böker, A. Müller, J. Augustin, C. Janowitz, and R. Manzke, Phys. Rev. B **60**, 4675 (1999).
[30] A.R. Beal and H.P. Hughes, J. Phys. C **12**, 881 (1979).
[31] A.R. Beal, W.Y. Liang, and H.P. Hughes, J. Phys. C **9**, 2449 (1976).
[32] Th. Finteis, M. Hengsberger, Th. Straub, K. Fauth, R. Claessen, P. Auer, P. Steiner, S. Hüfner, P. Blaha, M. Vögt, M. Lux-Steiner, and E. Bucher, Phys. Rev. B **59**, 2461 (1999).
[33] M. Tanaka, H. Fukutani, and G. Kuwabara, J. Phys. Soc. Jpn. **45**, 1899 (1978).
[34] Y. Onodera and Y. Toyozawa, J. Phys. Soc. Jpn. **22**, 833 (1967).
[35] V. Langglais, H. Belkhir, J.-M. Themlin, J.-M. Debever, L.-M. Yu, and P.A. Thiry, Phys. Rev. B **52**, 12 095 (1995).
[36] M. Sancrotti, L. Braicovich, C. Chemelli, and G. Trezzi, Solid State Commun. **66**, 593 (1988).
[37] D. Voß, P. Krüger, A. Mazur, and J. Pollmann, Phys. Rev. B **60**, 14 311 (1999).
[38] Just below -1 eV a rather dispersionless emission feature is observed for all three compounds from Γ to about halfway to K. For $MoSe_2$ an equivalent, rather dispersionless state was reported (Ref. 10) and discussed in the context of a vibronic polaron similar to the electronic polaron claimed for $TiTe_2$ (Ref. 39). Recent studies (Ref. 40) on $TiTe_2$ disprove the electronic polaron concept so that also in the case of similar layered transition metal dichalcogenides other explanations may be more plausible. The respective peak in the ΓK series might be nondispersive simply due to a weak overlap with other mainly chalcogen derived orbitals in the direction close to the z-axis. With increasing off-normal emission angles ϑ, i.e., reaching the Brillouin zone edge, the small overlap with the chalcogen p_z orbitals gives rise to the observed dispersion.
[39] D.K.G. de Boer, C.F. van Bruggen, R. Coehoorn, C. Haas, G.A. Sawatzky, H.W. Myron, D. Norman, and H. Padmore, Phys. Rev. B **29**, 6797 (1984).
[40] R. Claessen, R.O. Anderson, G.-H. Gweon, J.W. Allen, W.P. Ellis, C. Janowitz, C.G. Olson, Z.X. Shen, V. Eyert, M. Skibowski, K. Fiemelt, and E. Bucher, Phys. Rev. B **54**, 2453 (1996).